Supporting Information

Unique Ligand Effect in Pt-Based Core-Shell Nanocubes to Boost Oxygen Reduction Electrocatalysis

Xingqiao Wu,[a,‡] XinKai Chen,[a,b,‡] Xiao Li,[a] Yucong Yan,[a,d] Jingbo Huang,[a] Junjie Li,[a] Rong Shen,[a] He Tian[a,b,*], Deren Yang[a] and Hui Zhang [a,c,*]

[a]*State Key Laboratory of Silicon Materials, School of Materials Science and Engineering, Zhejiang University, Hangzhou, Zhejiang 310027, People's Republic of China*
[b]*State Key Laboratory of Silicon Materials and Center of Electron Microscopy, School of Materials Science & Engineering, Zhejiang University, Hangzhou, Zhejiang 310027, People's Republic of China*
[c]*Institute of Advanced Semiconductors, Hangzhou Innovation Center, Zhejiang University, Hangzhou, Zhejiang 310027, People's Republic of China*
[d]*BTR New Material Group CO., LTD., GuangMing District, Shenzhen 518106, China.*

‡These authors contributed equally
*Corresponding author. E-mail: msezhanghui@zju.edu.cn, hetian@zju.edu.cn.

1. Materials and Computational Method.

1.1. Chemicals.

Palladium(II) acetylacetonate ($Pd(acac)_2$, 99%), lead(II) acetylacetonate ($Pb(acac)_2$, technical grade), chloroplatinic(IV) acid ($H_2PtCl_6 \cdot xH_2O$, 99.9%), n-butylamine (98%), potassium hydroxide (KOH, 99.99%) were all purchased from Sigma Aldrich. Commercial Pt/C (20 wt%) was purchased from Alfa Aesar. Oleylamine (OAm, 80%-90%) was purchased from Aladdin. Ethanol, cyclohexane and chloroform were purchased from Sinopharm Chemical Reagent. All the chemicals and materials were used as received. All aqueous solutions were prepared using ultrapure water with a resistivity of 18.2 MΩ·cm.

1.2. Computational Method.

All the density functional theory (DFT) calculations were performed by using Vienna Ab-initio Simulation Package[1,2] (VASP) under the Projected Augmented Wave[3] (PAW) method. The revised Perdew-Burke-Ernzerhof (RPBE) functional was used to describe the exchange and correlation effects, since it has proved to provide useful trend in computing adsorption energies.[4-6] In all the calculations, the cut-off energy was set to be 500 eV. The (100) surface was simulated to represent the catalytic interface. The Monkhorst-Pack grid [7] were set to be 3×3×1 and 6×6×1 for computing the adsorption energy and d-band centre, respectively. A 15 Å vacuum layer was applied in z-direction of the slab models, preventing the slabs from vertical interactions.

The oxygen adsorption energy (ΔE_O) was defined as:

$$\Delta E_O = E_{slab+O} - E_{slab} - E_O$$

where E_{slab+O} is the energy of slab model with an adsorbed oxygen atom, E_{slab} is the energy

of the clean slab, and E_O is the energy of an oxygen atom referenced as (H_2O–H_2). Under this definition, a smaller value of ΔE_O indicates a stronger adsorption.

2. Supporting Figures and Tables.

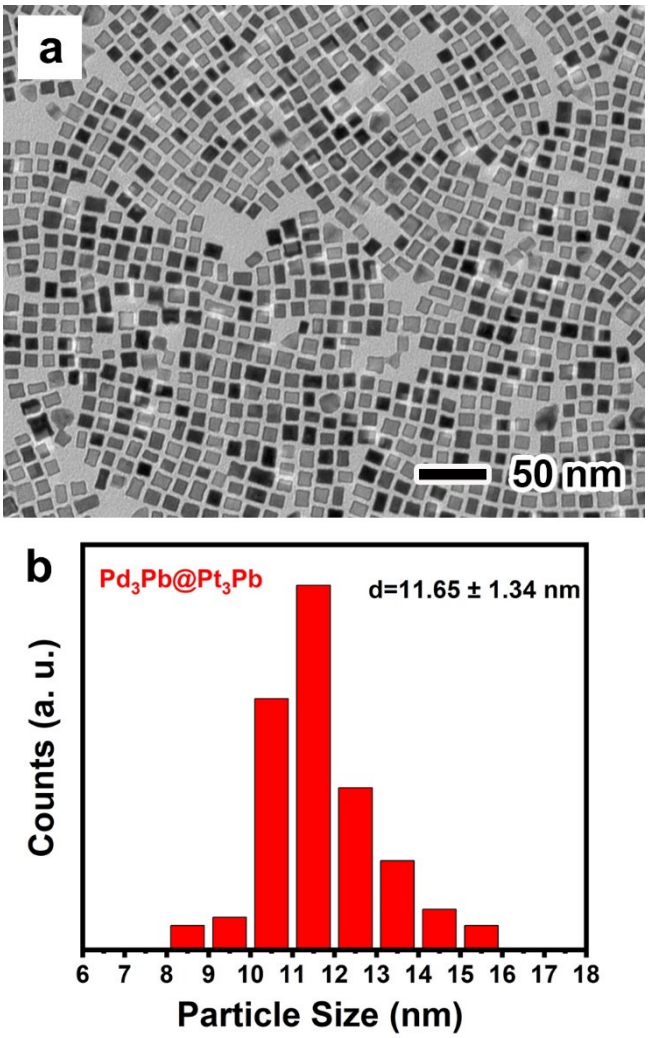

Fig. S1. (a) TEM images and (b) corresponding size distribution of the $Pd_3Pb@Pt_3Pb$ nanocubes.

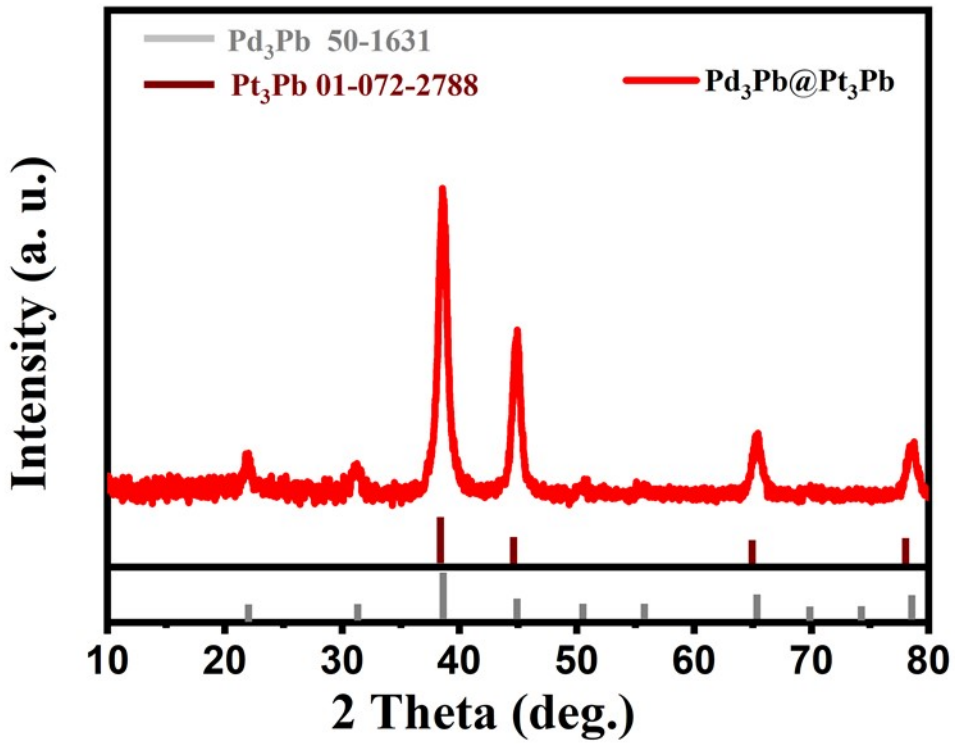

Fig. S2. XRD pattern of the $Pd_3Pb@Pt_3Pb$ nanocubes.

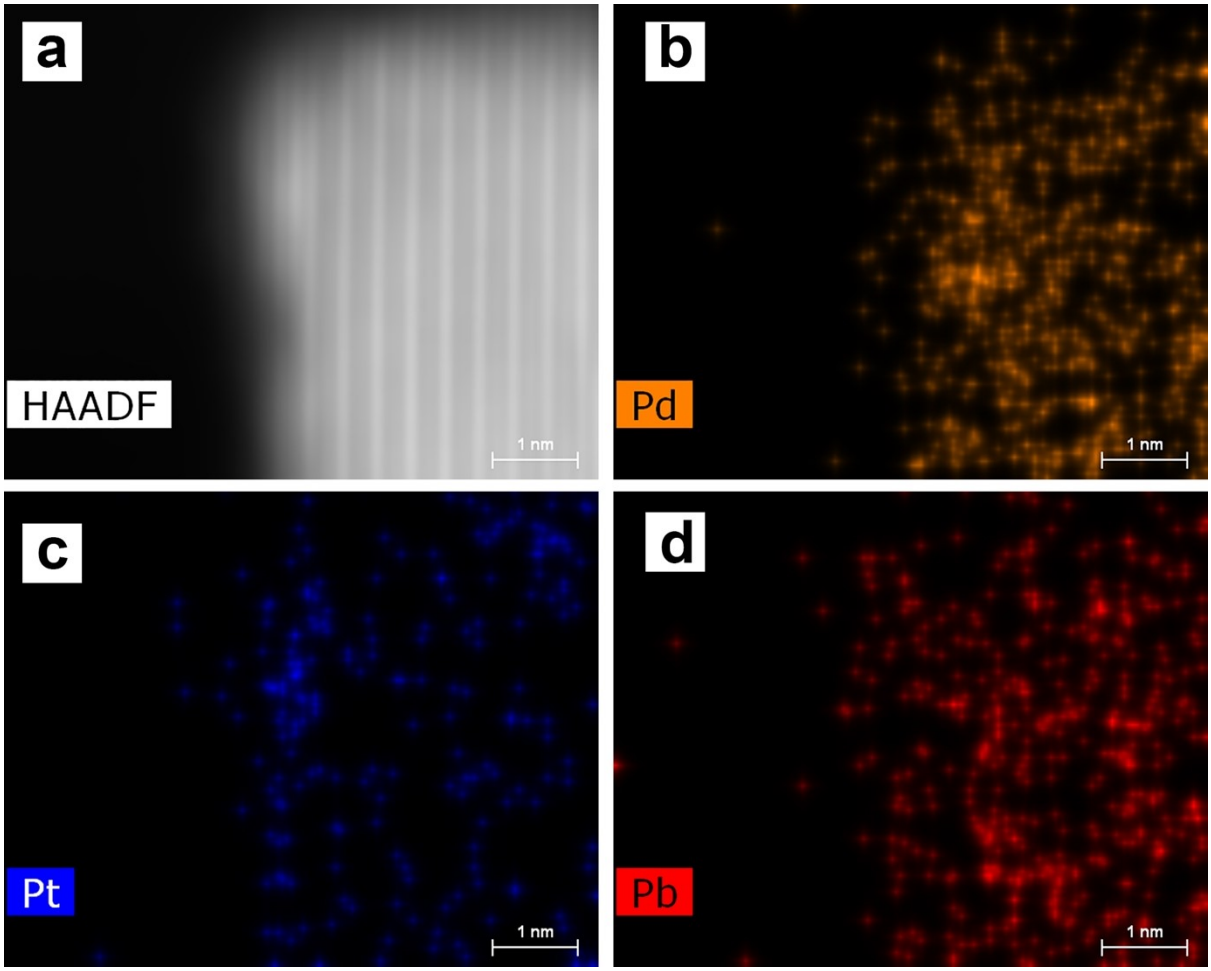

Fig. S3. High-magnified EDX mapping image of the surface of the $Pd_3Pb@Pt_3Pb$ nanocubes.

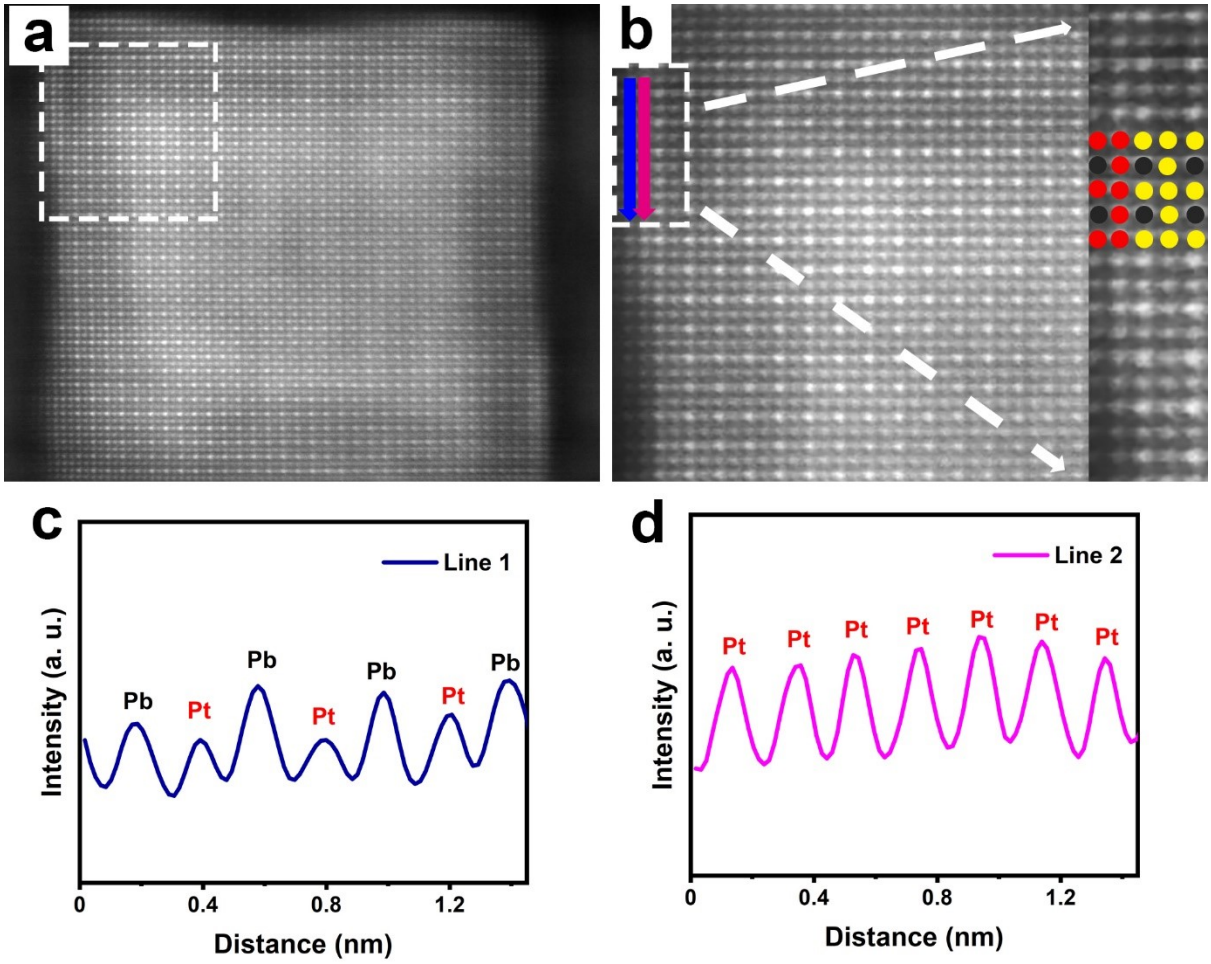

Fig. S4. (a,b) Aberration-corrected HAADF-STEM images of the $Pd_3Pb@Pt_3Pb$ nanocubes and (c,d) corresponding line profiles of intensity of atoms along the directions marked in (b).

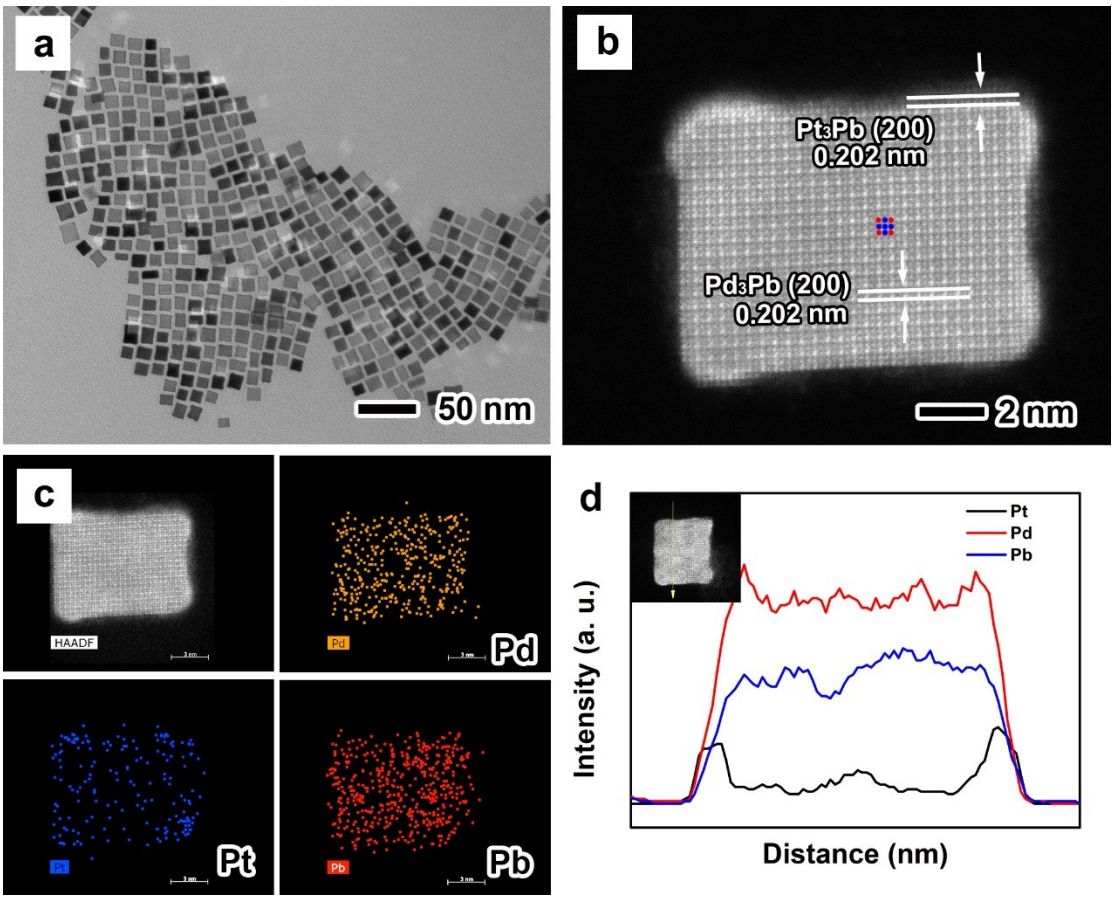

Fig. S5. (a) TEM image, (b) aberration-corrected HAADF-STEM image, (c) EDX mapping image and (d) line-scan profiles of the $Pd_3Pb@Pt_4Pb$ nanocubes.

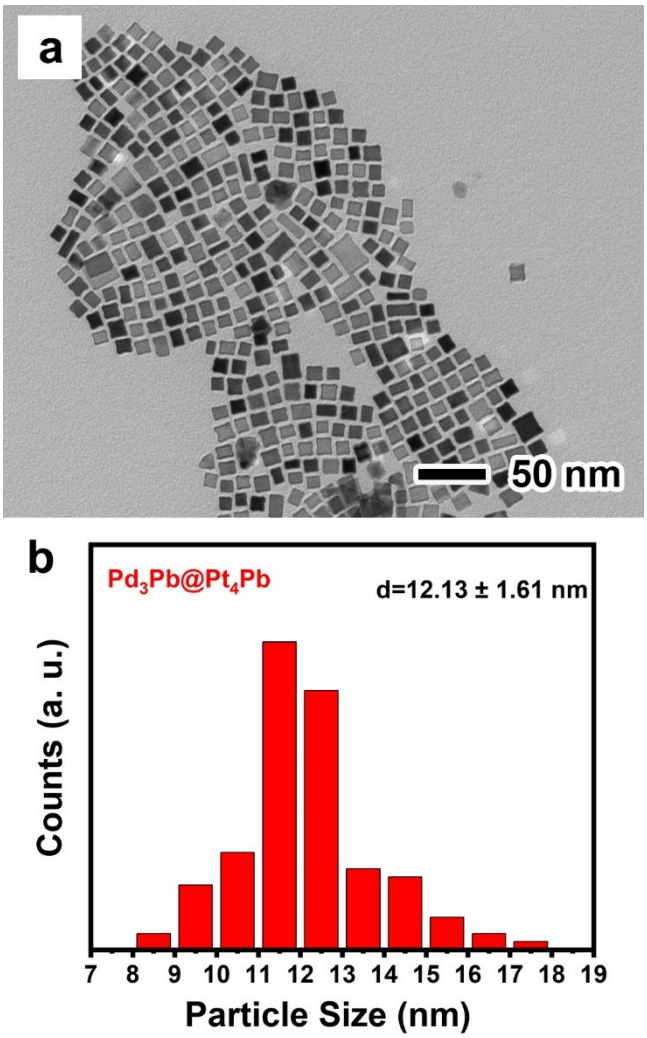

Fig. S6. (a) TEM image and (b) corresponding size distribution of the $Pd_3Pb@Pt_4Pb$ nanocubes.

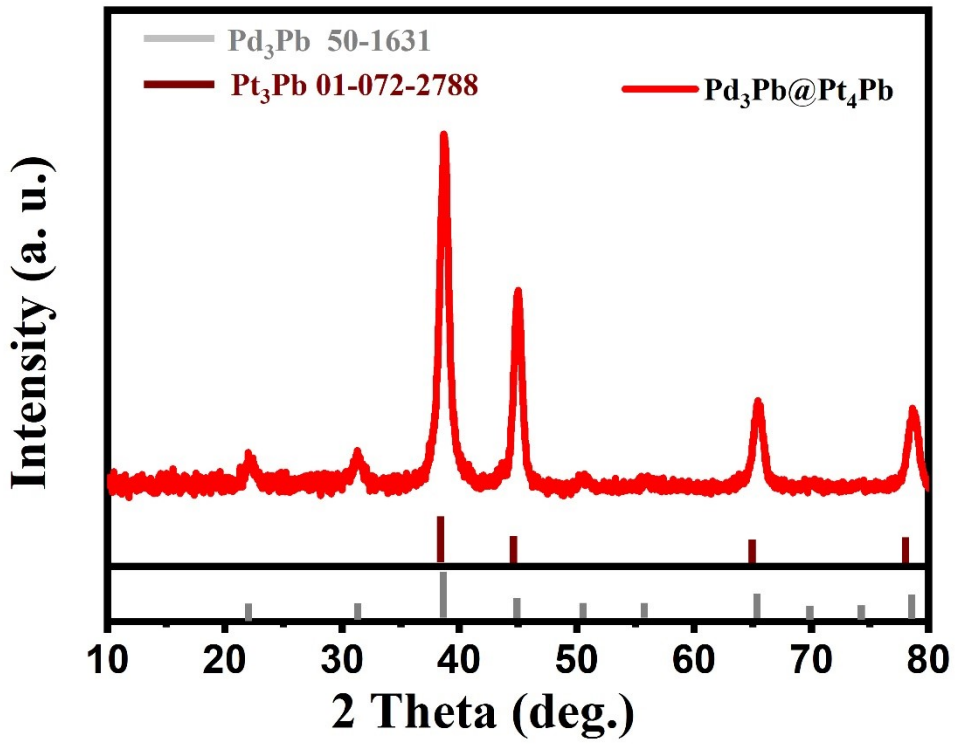

Fig. S7. XRD pattern of the $Pd_3Pb@Pt_4Pb$ nanocubes.

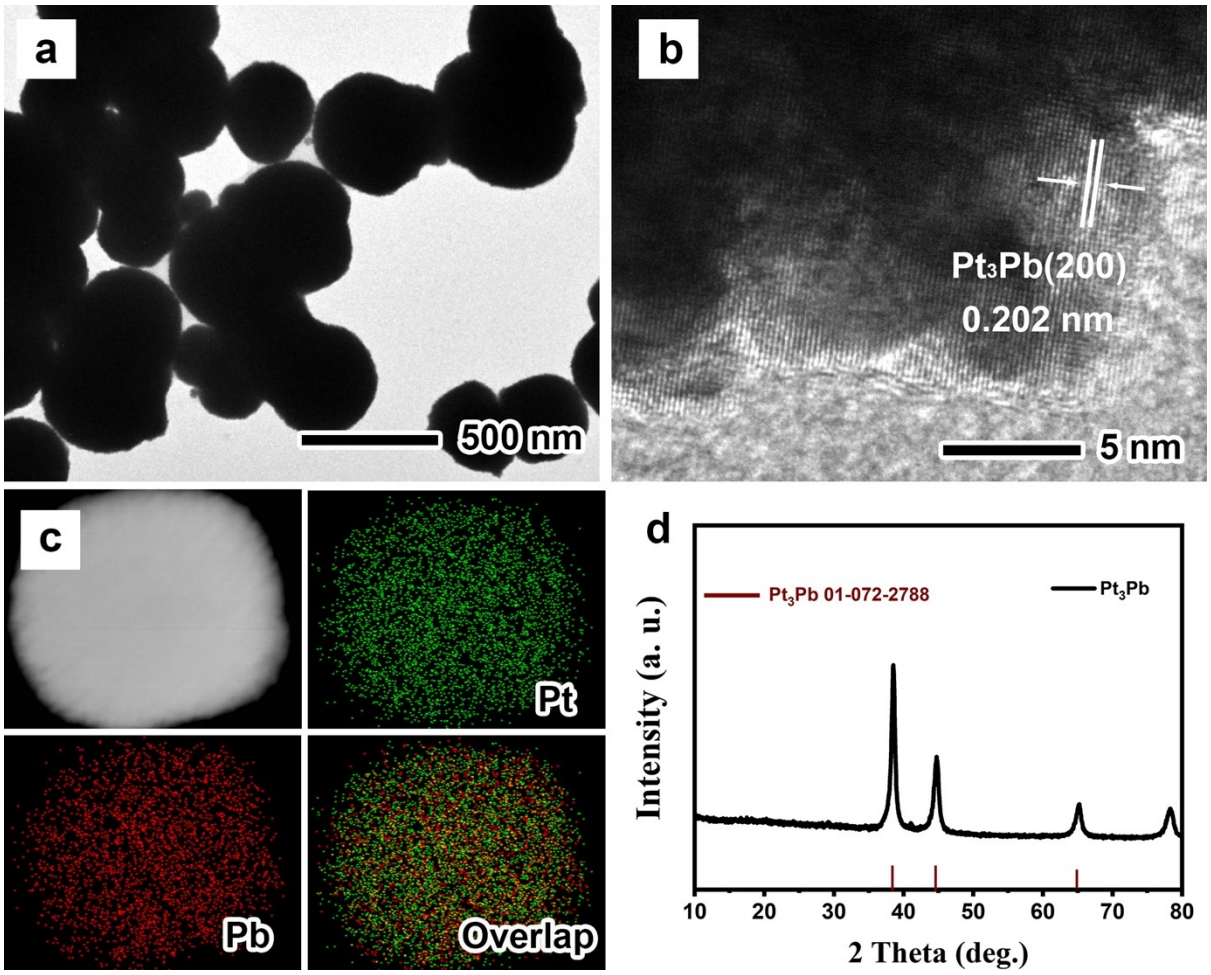

Fig. S8. (a) TEM image, (b) HRTEM image, (c) EDX mapping image and (d) XRD pattern of the Pt_3Pb nanoparticles.

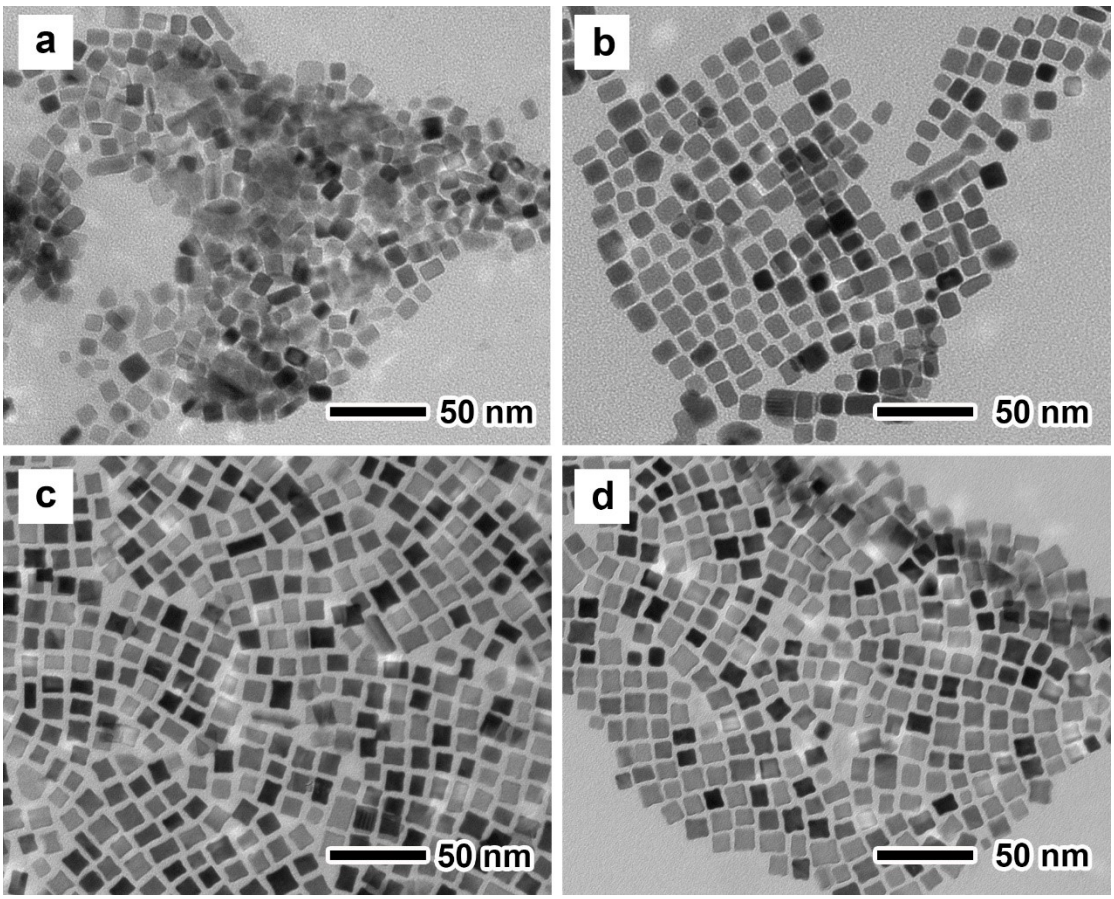

Fig. S9. TEM images of the Pd_3Pb/Pt_3Pb prepared using the standard procedure at different reaction times: (a) 3, (b) 5, (c) 10, and (d) 20 min.

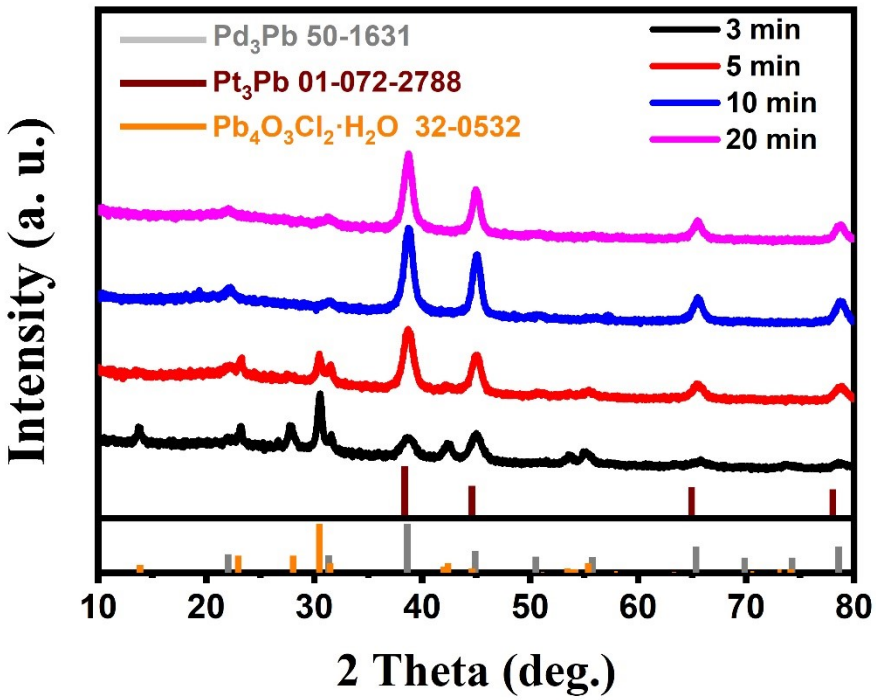

Fig. S10. XRD patterns of the Pd_3Pb@Pt_3Pb prepared using the standard procedure at different reaction times: (a) 3, (b) 5, (c) 10, and (d) 20 min.

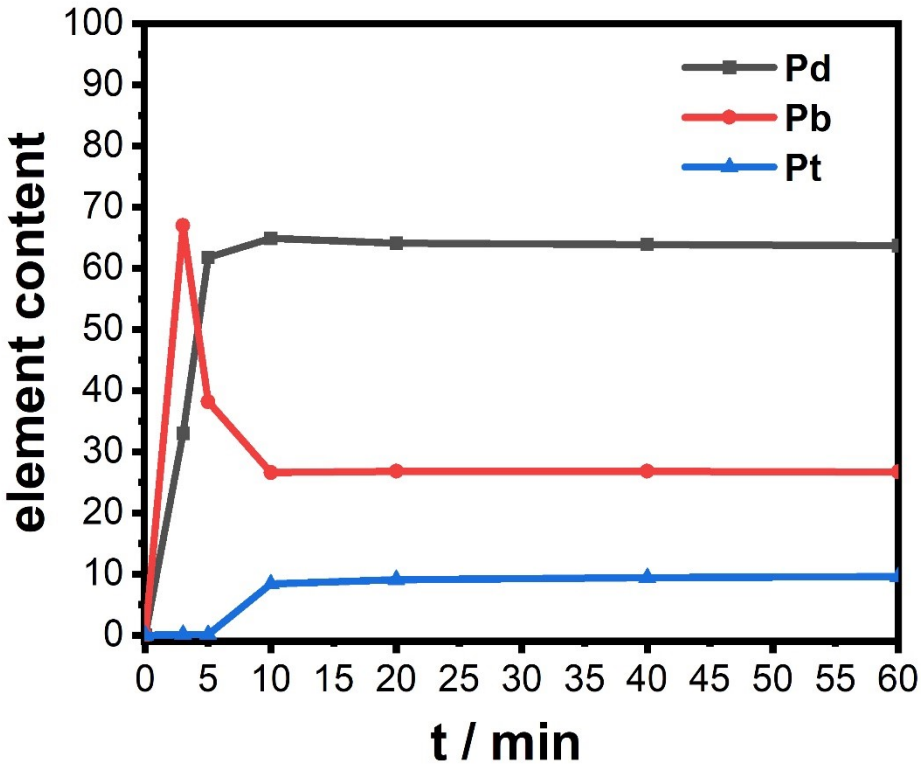

Fig. S11. Change in mol % of Pt, Pd and Pb during the reaction for the synthesis of the $Pd_3Pb@Pt_3Pb$ nanocubes.

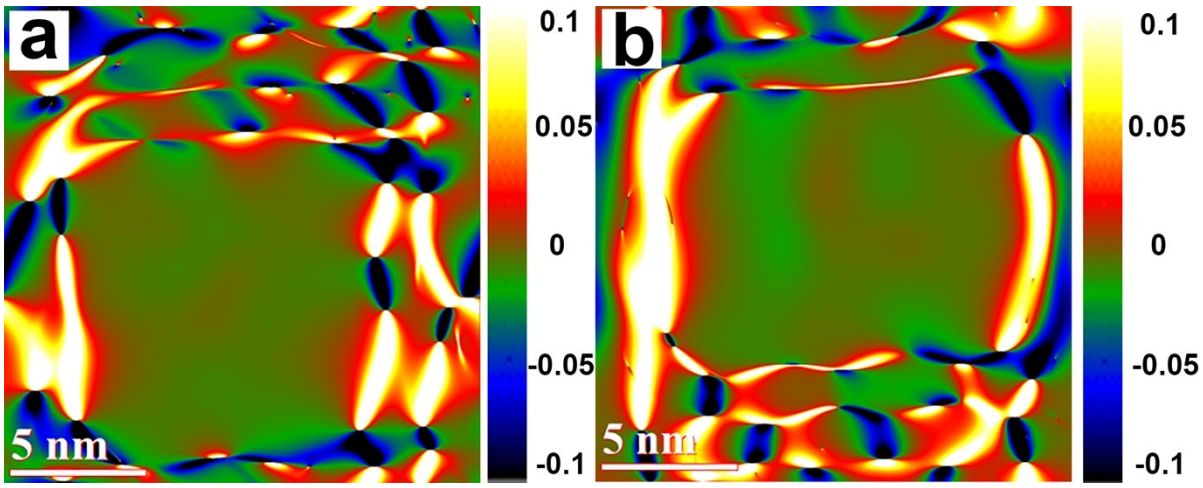

Fig. S12. Strain distribution determined by GPA. (a) Mapping image of ε_{xx} distribution of Figure 2a. (b) Mapping image of ε_{xx} distribution of Figure 13a

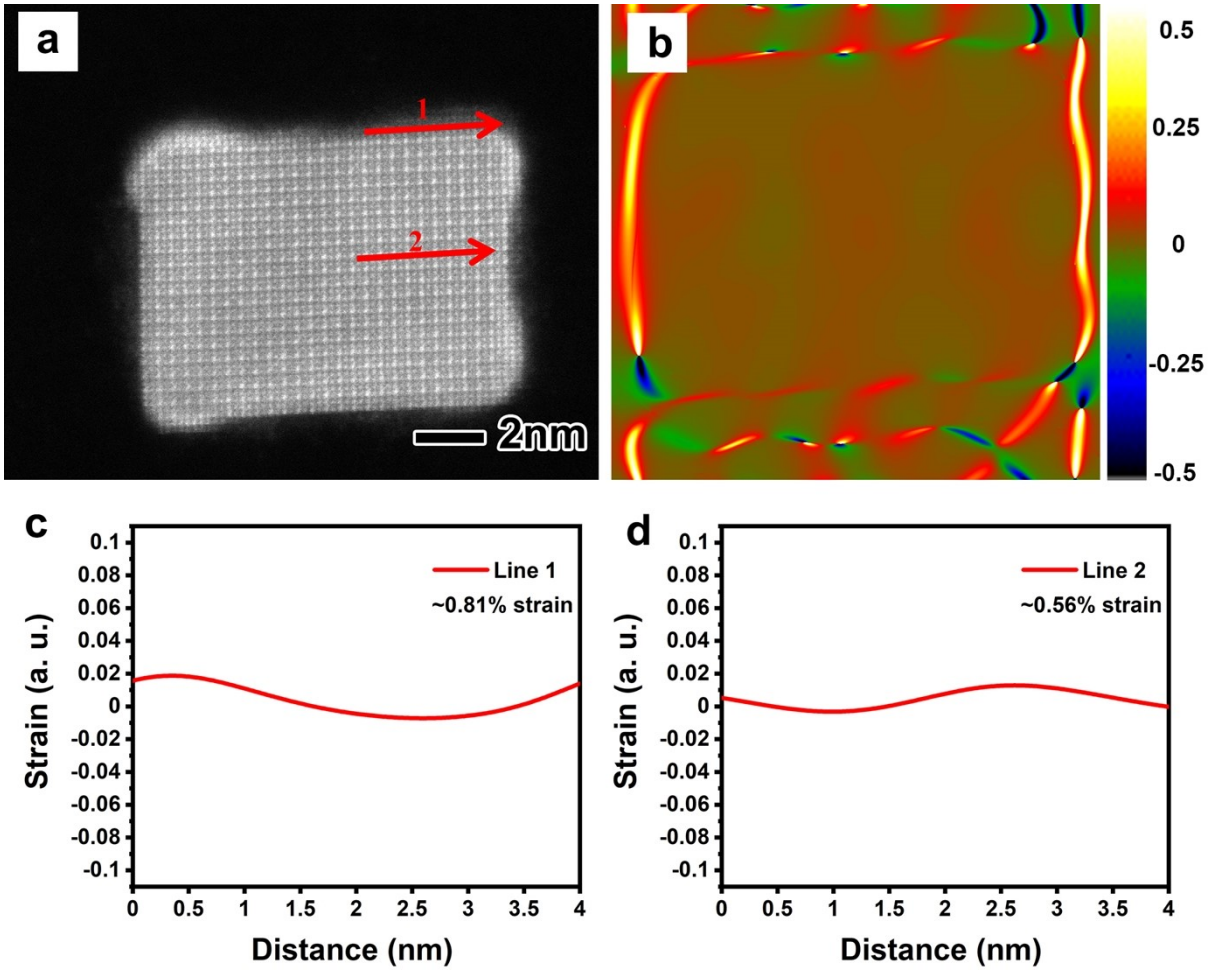

Fig. S13. Strain distribution of the $Pd_3Pb@Pt_4Pb$ nanocubes determined by GPA. (a) Aberration-corrected HAADF-STEM image of a $Pd_3Pb@Pt_4Pb$ nanocube. (b) Mapping image of ε_{xx} distribution of (a). (c) and (d) Line profiles of ε_{xx} along directions marked in (a).

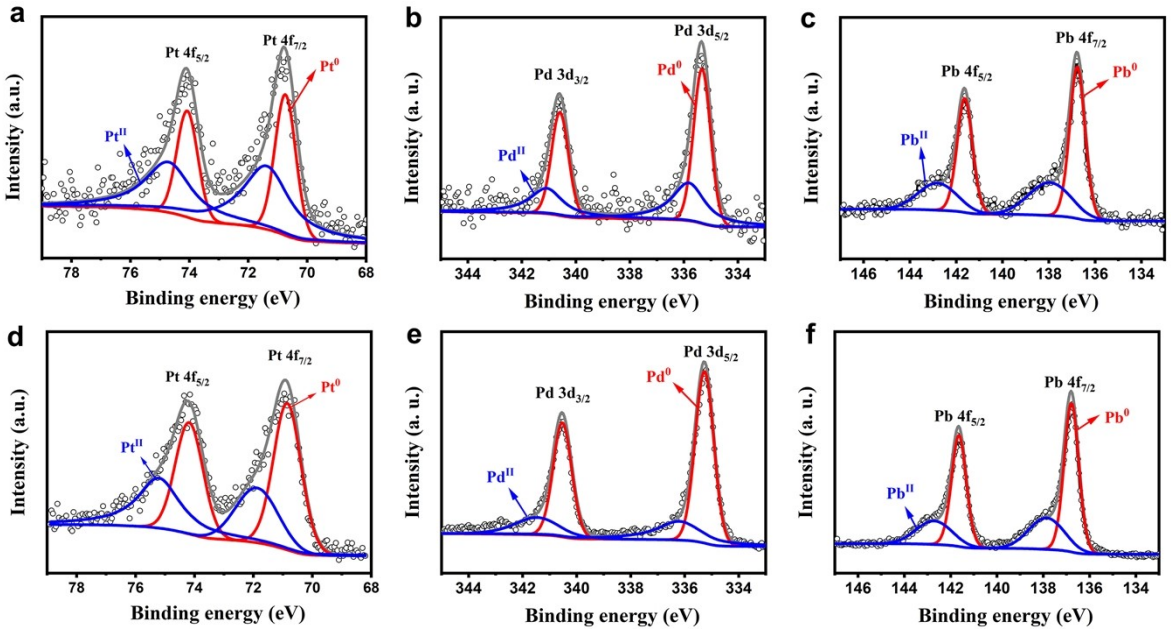

Fig. S14. (a, d) Pt 4f, (b, e) Pd 3d and (c, f) Pb 4f XPS spectra of the $Pd_3Pb@Pt_3Pb$ and $Pd_3Pb@Pt_4Pb$ nanocubes, respectively.

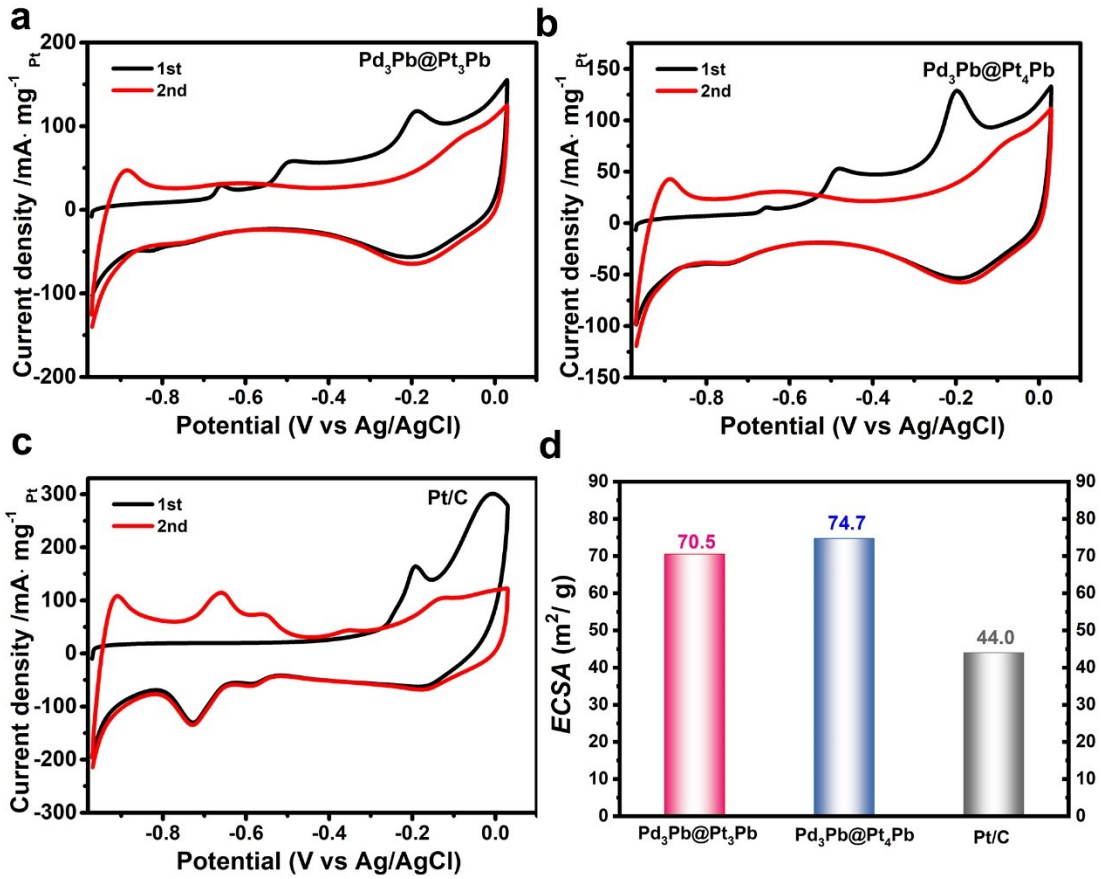

Fig. S15. CO stripping curves of three catalysts recorded in 0.1 M KOH solution at a sweep rate of 50 mV/s: (a) $Pd_3Pb@Pt_3Pb$ nanocubes, (b) $Pd_3Pb@Pt_3Pb$ nanocubes, and (c) Pt/C. (d) A comparison of ECSAs of these three catalysts.

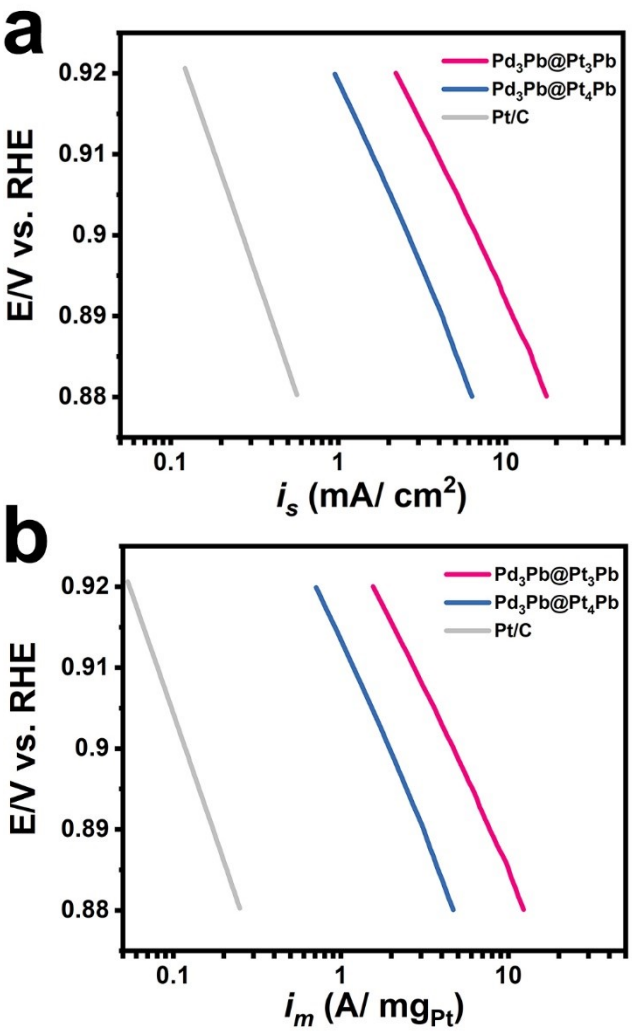

Fig. S16. (a) Area-specific (i_s, mA/cm^2) and (b) mass (i_m, A/mg$_{Pt}$) ORR activities for Pd$_3$Pb@Pt$_3$Pb nanocubes, Pd$_3$Pb@Pt$_4$Pb nanocubes and Pt/C reference catalysts.

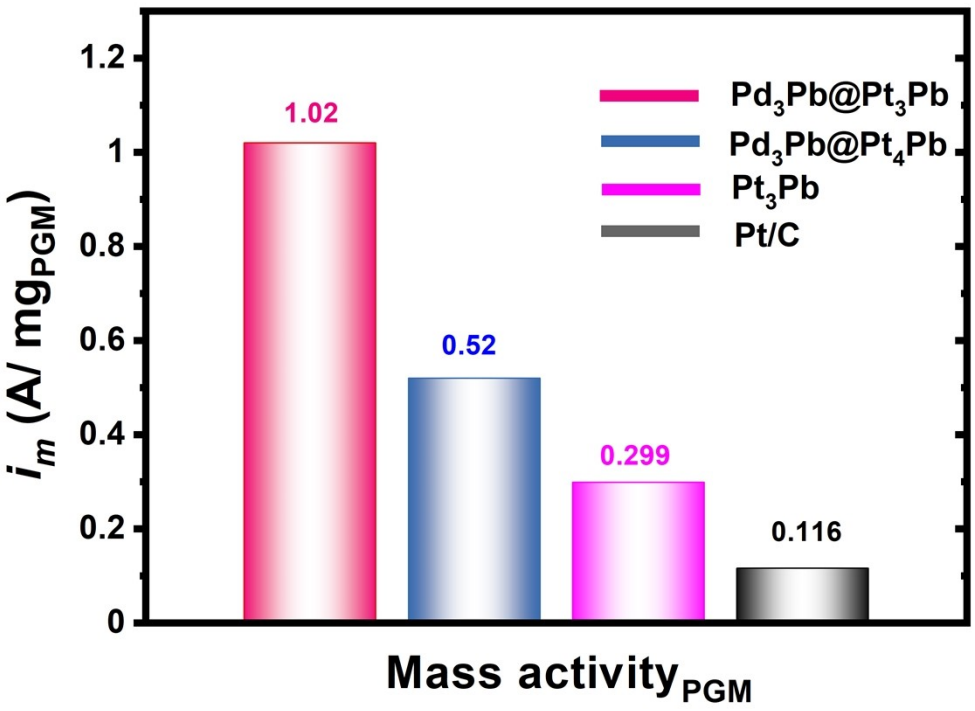

Fig. S17. Mass activities (normalized by the mass of PGM, i_m, A/mg_{PGM}) of the $Pd_3Pb@Pt_3Pb$ nanocubes, $Pd_3Pb@Pt_4Pb$ nanocubes, Pt_3Pb nanoparticles and commecial Pt/C catalysts for ORR.

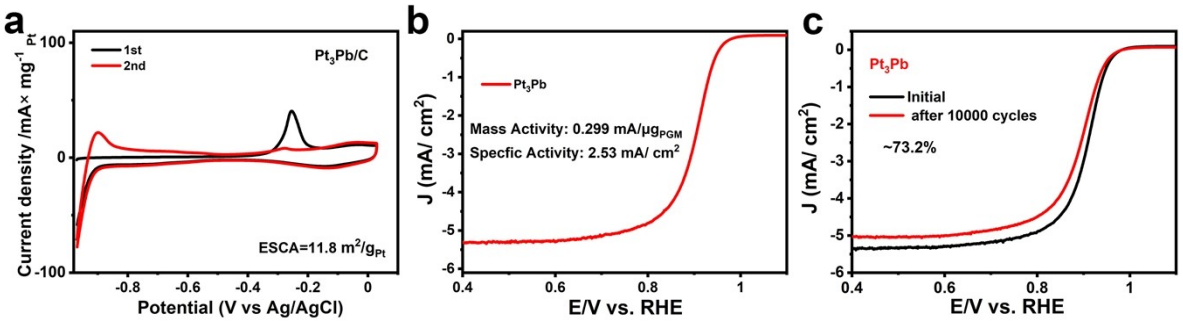

Fig. S18. (a) CO stripping curves, (b) mass (i_m, A/mg$_{Pt}$) and area-specific (i_s, mA/cm^2) activities, and (c) ORR polarization curves before and after 10000 cycles between 0.6 and 1.0 V at a scan rate of 100 mV/ s versus RHE of the Pt_3Pb/C catalysts.

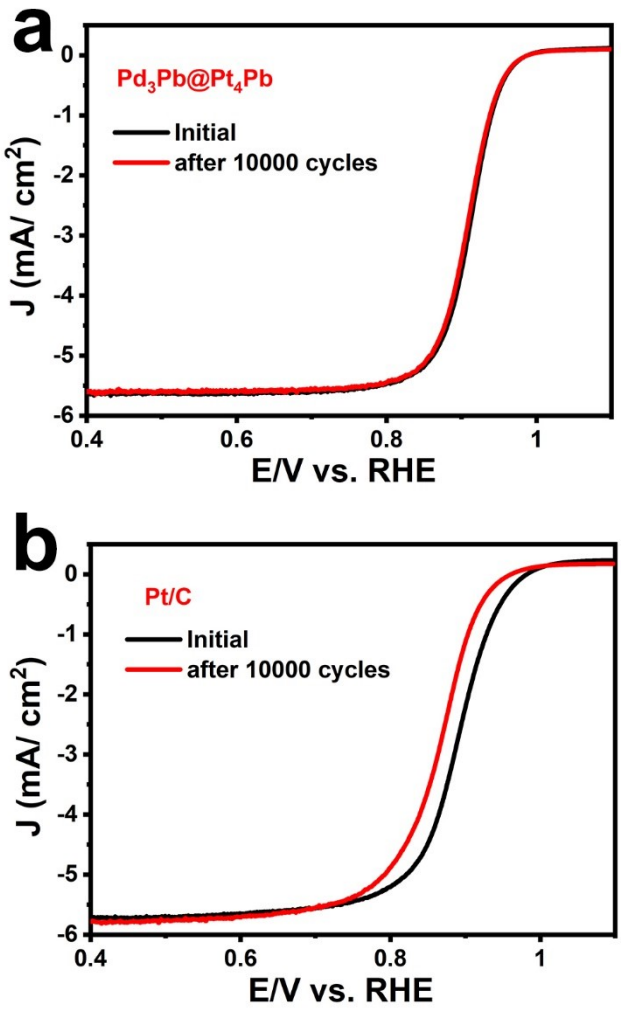

Fig. S19. ORR polarization curves of (a) $Pd_3Pb@Pt_4Pb$ nanocubes/C and (b) commercial Pt/C catalysts before and after 10000 cycles between 0.6 and 1.0 V at a scan rate of 100 mV/ s versus RHE.

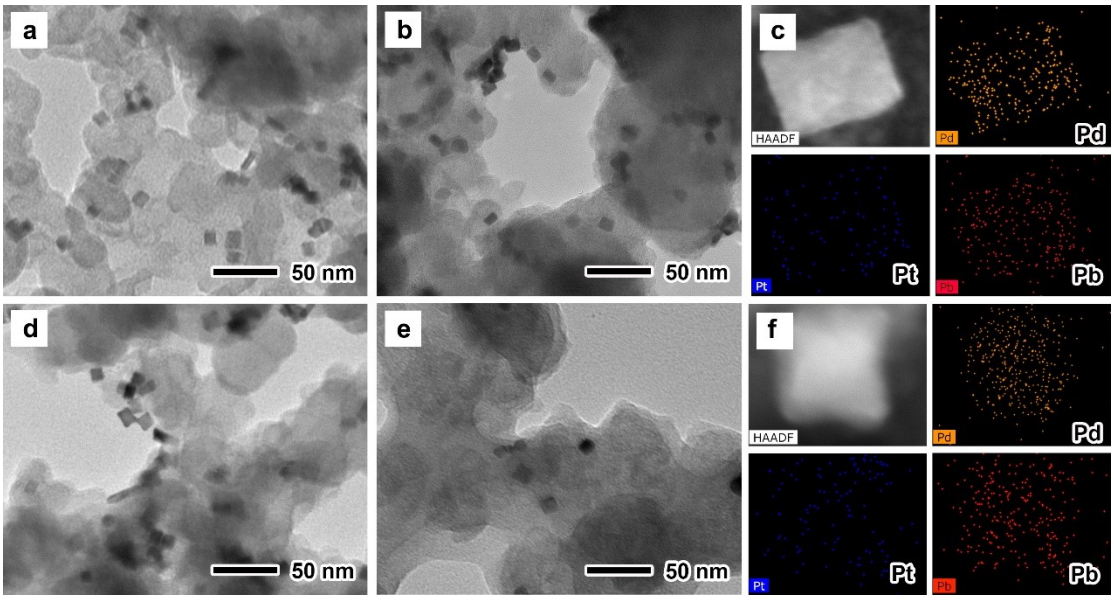

Fig. S20. TEM and HAADF-STEM-EDX mapping characterizations of (a-c) $Pd_3Pb@Pt_3Pb$ nanocubes/C and (d-f) $Pd_3Pb@Pt_4Pb$ nanocubes/C before and after 10000 cycles ADT test.

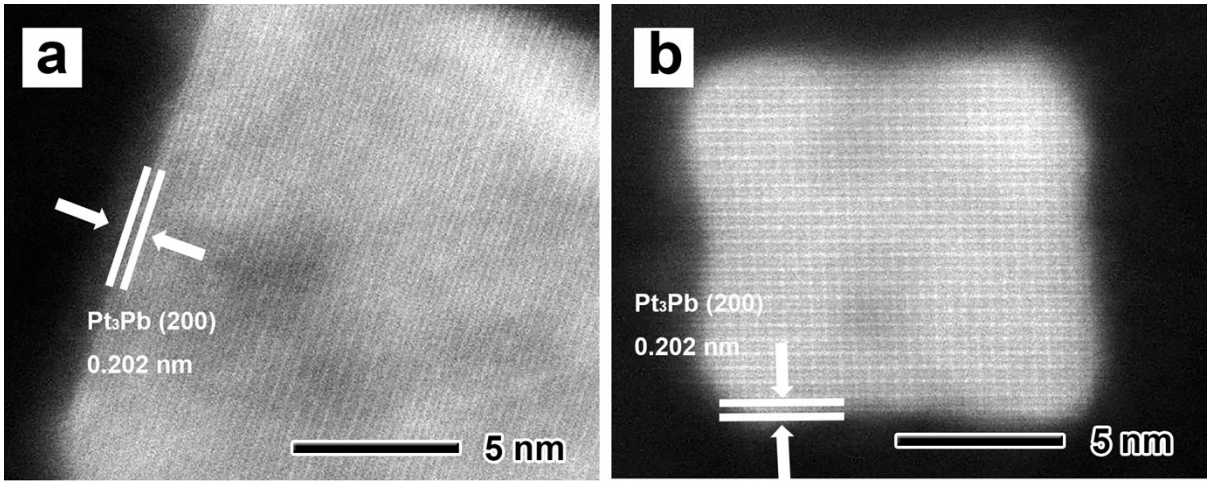

Fig. S21. HAADF-STEM images of (a,b) two Pd_3Pb@Pt_3Pb/C samples after ADT.

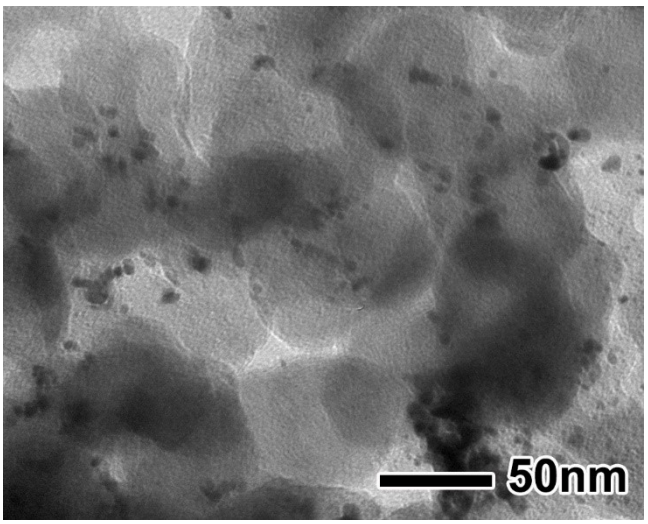

Fig. S22. TEM image of the commercial Pt/C catalyst after 10000 cycles ADT test.

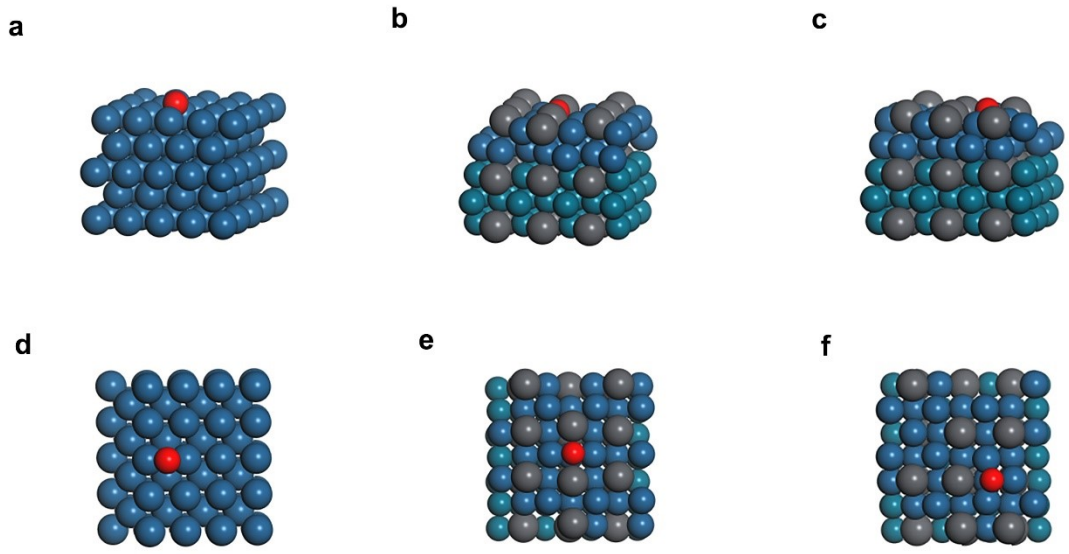

Fig. S23. DFT models of (a) Pt(100), (b) $Pd_3Pb@Pt_3Pb(100)$, and (c) $)Pd_3Pb@Pt_4Pb(100)$.

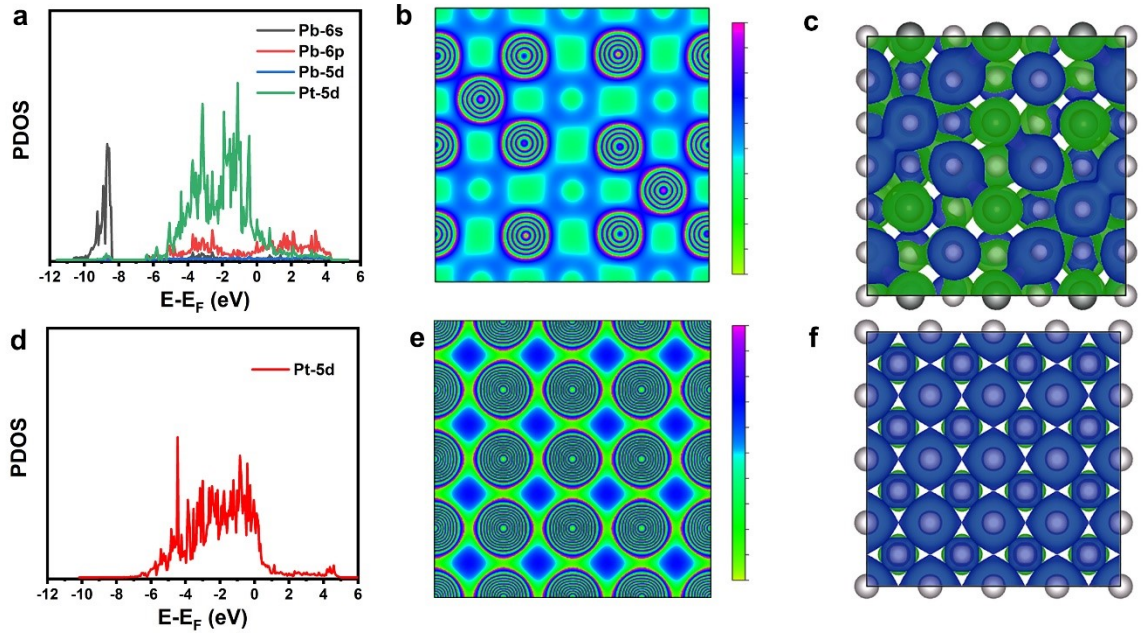

Fig. S24. DFT calculations. The PDOS of (a) $Pd_3Pb@Pt_4Pb$ and (d) Pt slab. The electron localization function analysis of surface in (b) $Pd_3Pb@Pt_4Pb$ slab and (e) Pt slab. The differential charge distributions for (c) $Pd_3Pb@Pt_4Pb$ slab and (f) Pt slab.

Table S1. ICP-AES data of $Pd_3Pb@Pt_3Pb$ and $Pd_3Pb@Pt_4Pb$ nanocubes.

Samples	Atomic ratio of Pd %	Atomic ratio of Pt %	Atomic ratio of Pb %	Pt/Pb*
$Pd_3Pb@Pt_3Pb$	63.7	9.6	26.7	3.1
$Pd_3Pb@Pt_4Pb$	62.0	12.1	25.9	4.1
Pt_3Pb	/	74.3	25.7	2.9

* Pt/Pb is defined as the atomic ratio of Pt and Pb after subtracting the amount of Pb in the Pd_3Pb cores with a Pd/Pb atomic ratio of 2.7:1.

Table S2. Summarized XPS data of $Pd_3Pb@Pt_3Pb$, $Pd_3Pb@Pt_4Pb$, Pt bulk, Pb bulk and Pd bulk.

Samples	Pt^0 $4f_{7/2}$	Pt^0 $4f_{5/2}$	Pb^0 $4f_{7/2}$	Pb^0 $4f_{7/2}$	Pd^0 $3d_{5/2}$	Pd^0 $3d_{3/2}$	Pt/Pb
$Pd_3Pb@Pt_3Pb$	70.74 eV	74.07 eV	136.77 eV	141.63 eV	335.33 eV	340.59 eV	0.76
$Pd_3Pb@Pt_4Pb$	70.85 eV	74.18 eV	136.78 eV	141.64 eV	335.27 eV	340.53 eV	1.05
Pb bulk	/	/	136.90 eV	141.76 eV	/	/	/
Pd bulk	/	/	/	/	335.1 eV	340.36 eV	/
Pt bulk	71.20 eV	74.53 eV	/	/	/	/	/

Table S3. Comparison of ORR performance of $Pd_3Pb@Pt_3Pb$ in this work with state of art electrocatalysts in the literatures.

Samples	i_m (A/mg_{Pt})	i_s (mA/cm^2)	Ref.
$Pd_3Pb@Pt_3Pb$	4.69	6.69	This work
$Pt_{37}Cu_{56}Au_7$ porous film	0.871	1.85	8
Pt−Pd binary superlattices	~2.1	~1.9	9
$Pd_{72}Pt_{28}$ alloy	/	1.249	10
H-Pt/$CaMnO_3$	0.38 (0.85V)	1.06 (0.85V)	11
CuPt-NC	0.32	0.47	12
NiPt TONPs	0.44	0.51	13
Pt-coated Pd nanocubes	/	0.708	14
Pt@Fe-N/R3DG	/	2.22	15
13% PtPdNT	0.333	1.48	16

Table S4. Summarized E_{ads+O}, E_{slab}, E_O, and ΔE_O for three kinds of surfaces including *fcc*-structured $Pd_3Pb@Pt_4Pb(100)$, $Pd_3Pb@Pt_3Pb(100)$, and Pt(100) obtained by DFT calculations.

Samples	**E_{slab+O} (eV)**	**E_{slab} (eV)**	**E_O (eV)**	**ΔE_O (eV)**
Pt(100)	-417.19	-411.39	-7.16	1.36
$Pd_3Pb@Pt_4Pb(100)$	-416.40	-410.62	-7.16	1.38
$Pd_3Pb@Pt_3Pb(100)$	-414.29	-408.58	-7.16	1.45

Table S5. Summarized position of d-band center for three kinds of surfaces including *fcc*-structured $Pd_3Pb@Pt_4Pb(100)$, $Pd_3Pb@Pt_3Pb(100)$, and Pt(100) obtained by DFT calculations.

Samples	**$E-E_F$ (eV)**
Pt(100)	-1.909
$Pd_3Pb@Pt_4Pb(100)$	-2.051
$Pd_3Pb@Pt_3Pb(100)$	-2.077

3. References

[1] G. Kresse and J. Furthmüller, *Phys. Rev. B* **1996**, *54*, 11169−11186.

[2] G. Kresse and J. Hafner, *Phys. Rev. B* **1994**, *49* 14251−14269.

[3] P.Blöchl, *Phys. Rev. B* **1994**, *50*, 17953−17979.

[4] J. Perdew, K. Burke and M. Ernzerhof, *Phys. Rev. Lett*. **1996**, *77*, 3865−3868.

[5] Y. Zhang and W. Yang, *Phys. Rev. Lett.* **1998**, *80*, 890.

[6] B. Hammer, L. Hansen and J. Nørskov, *Phys. Rev. B* **1999**, *59*, 7413−7421.

[7] H. Monkhorst and J. Pack, *Phys. Rev. B* **1976**, *13*, 5188.

[8] Y. Xie, Y. Yang, D. Muller, H. Abruña, N. Dimitrov and J. Fang, *ACS Catal.* **2020**, *10*, 9967−9976.

[9] Y. Kang, X. Ye, J. Chen, Y. Cai, R. Diaz, R. Adzic, E. Stach and C. Murray, *J. Am. Chem. Soc.* **2013**, *135*, 42−45.

[10] K. Jukk, N. Kongi, K. Tammeveski, J. Solla-Gullo´n and J.. Feliu, *ChemElectroChem* **2017**, *4*, 2547–2555.

[11] X. Han , F. Cheng , T. Zhang , J. Yang , Y. Hu and J.Chen, *Adv. Mater.* **2014**, *26*, 2047–2051.

[12] V. Dhavale and S. Kurungot, *ACS Catal.* **2015**, *5*, 1445−1452.

[13] T. Xia, J. Liu, S. Wang, C. Wang, Y. Sun, L. Gu and R. Wang, *ACS Appl. Mater. Interfaces* **2016**, *8*, 10841−10849.

[14] C. Lee, C. Yang, C. Liu, Z. Liu and J. Ye, *J. Power Sources* **2014**, *268*, 712−717.

[15] Y. Qin, L. Chao, J. He, Y. Liu, F. Chu, J. Cao, Y. Kong and Y. Tao, *J. Power Sources* **2016**, *335*, 31−37.

[16] S. John, R. Atkinson III, O. Dyck, C. Sun, T. Zawodzinski Jr, and A. Papandrew, *Chem. Commun.* **2015**, *51*, 16633−16636.